Three Dimensional Behavior of Square Footing and Unlined Soft Ground Tunnel

정방형 기초와 Unlined Soft Ground 터널의 3차원적 거동

Yoo, Chung-Sik*
유 충 식

요 지

Lining이 타설되기 이전의 unlined 터널과 지상 구조물의 역학적 상호작용은 심각한 구조적 안정 문제를 야기시킬 수 있으며 이에 따른 피해를 최소화 하기 위해서는 unlined 터널과 인근 구조물의 역학적 상호작용에 관한 이해가 선행 되어져야 한다. 본 논문에서는 정방형 기초와 unlined 터널의 3차원적 거동에 관한 매개변수 변환연구의 결과를 다루었다. 연구를 위해서 3차원 탄소성 유한요소해석 프로그램을 개발하고 이를 이용하여 다양한 경계조건을 해석하였으며 기초의 극한 지지력, 지반과 터널주위의 응력 분포, 그리고 기초의 침하와 터널의 변형 등의 컴퓨터 해석 결과를 고찰하여 정방형 기초와 unlined 터널의 역학적 거동을 검토하였다. 그 결과 unlined 터널은 기초의 극한 지지력을 감소시키며 그 정도는 터널의 크기나 위치 뿐만이 아니라 기초의 형상이나 근입깊이 등에 의해서 영향을 받음을 알 수 있었다. 또한 정방형 기초 아래에 위치하는 터널은 터널의 축 방향으로 3차원적 응력을 받음을 알 수 있었으며 지반과 터널주위에 발생하는 응력의 크기는 정방형 기초의 경우가 연속 기초의 경우보다 현저히 작으며 그 차이는 위치와 응력의 종류에 따라 다른 것으로 밝혀졌다. 또한 기초의 파괴 mechanism은 기초와 터널의 상호작용의 정도에 따라 다름을 볼 수 있었다.

Abstract

Interaction between an unlined tunnel prior to lining installation and overlying structures may cause a serious stability problem. To minimize potential structural damage of both the tunnel and the overlying structures requires a thorough understanding of footing and unlined tunnel interaction mechanism. This paper presents the results of a parametric study on the three dimensional behavior of square footing and unlined tunnel. For analysis, a three dimensional elasto plastic finite element computer program was developed. Using the program, a wide range of boundary conditions were analyzed and the results of computer analysis such as stress distribution, ultimate bearing capacity, and footing settlement and tunnel deformation were used to evaluate the mechanistic behavior of square footing and unlined tunnel. The results indicate that the presence of an unlined tunnel reduces the ultimate bearing capacity of a footing, and the degree of reduction depends not only on the tunnel size and location but also the footing shape and embedment depth. Also

* 정회원, 성균관대학교 토목공학과 조교수

revealed is that an unlined tunnel under a square footing is subjected to three dimensional stress pattern along the tunnel axis, and that the magnitudes of stresses in the foundation soil and around tunnel perimeter are considerably smaller when loaded with a square than with a strip footings and the difference varies with the location and the type of stress. It is also revealed that the footing failure mechanism varies with the degree of footing and tunnel interaction.

1. Introduction

Transportation, water, and sewer tunnels as well as utility conduits are often constructed in soft ground. When a tunnel is present underground, the performance of footings of overlying structures may be seriously affected due to the interaction between the tunnel and the footings. In addition, the footing load together with the sustained overburden pressure may impose a threat to the tunnel stability. Although soft ground tunnels are lined eventually, the most critical period with respect to the stability of both the footing and the tunnel itself is before lining installation when the tunnel is left unsupported. To date, no rational method of stability analysis for footing-unlined tunnel system has been formulated, which will lead to a safe and economical design of footing-tunnel system. To develop such a methodology requires a thorough understanding of footing and unlined tunnel interaction mechanism.

Over the years, the subject of footing and tunnel/cavity interaction has been tackled by means of the numerical method of analysis[1, 2, 3, 11, 12, 13, 14]. A great majority of the available studies, however, are focused on two-dimensional plane strain loading condition, and as a result, the findings from the previous studies are applicable to tunnels loaded with a strip footing only. Therefore, the three dimensional behavior of square footing-unlined tunnel system was investigated using a developed three-dimensional elasto-plastic finite element computer program with the aim of understanding the interaction mechanism between a footing and an unlined tunnel and also establishing a data base for future development of a stability analysis method for footing-tunnel system.

2. Three-Dimensional Finite Element Formulation

The developed three-dimensional finite element computer program adopts the isoparametric hexahedral element with 8 nodes and employs the basic techniques required for simulating non linear soil behavior, such as incremental stress-strain relationships and the computational techniques used in implementing the constitutive law for elasto-plastic behavior. In addition, a blocked out-of-core algorithm is incorporated in order to handle large size of global stiffness matrix. The computer program consists of three parts:a pre-processor, the

main program, and a post-processor. The pre-processor is used to facilitate the finite element mesh generation, and the post-processor is for presenting the results of finite element analysis in desired graphical forms. The following paragraphs describe the basic formulations employed in the program.

2.1 Finite Element Model

In the developed program, the non linear elastic behavior of soil is modeled by the hyperbolic stress-strain relation proposed by Duncan and Chang[8]. Since the material parameters change with the state of stress in nonlinear elastic behavior, the incremental approach, which approximates the nonlinear behavior as piecewise linear, is used. During the application of each load increment, the material is considered to be linear and elastic, but different material properties are used for different increments. In each increment of load, the stress increment is related to the strain increment through the use of tangential stiffness modulus(E_t) which is defined as below:

$$E_t=[1-\frac{R_f(1-\sin\phi)(\sigma_1-\sigma_3)}{2c\cos\phi+2\sigma_3\sin\phi}]^2 KP_a(\frac{\sigma_3}{P_a})^n \tag{1}$$

where R_f is the ratio of ultimate to failure deviatoric stresses, ranging from 0.7 to 1.0, P_a is atmospheric pressure, and K and n are material constants.

Elasto-Plastic behavior of soil is described by Drucker-Prager yield criterion[7] given in Eq. (2) in conjunction with the Reye's incremental stress-strain relationship.

$$f=f(J_1, J_{2D})=\sqrt{J_{2D}}-\alpha J_1-k \tag{2}$$

where J_1 and J_{2D} are the first and the second invariants of stress tensor. α and k in above equation are the material constants which are expressed in terms of angle of internal friction (ϕ) and cohesion(c).

The yield criterion given in Eq. (2) and the flow rule of plasticity form the basis of the incremental elasto-plastic stress-strain relation. The movement of the point representing the values of the principal stresses at any instant in the principal stress space can be used to describe the response of an elasto-plastic material to a given loading. Only elastic deformations occur when the point moves within the space bounded by the yield surface. As soon as the stress point reaches the yield surface, yielding occurs, and any movement of the point on the yield surface produces both elastic and plastic deformations. These two cases can be explained using the aforementioned yield function.

a) If $f < k$ and $df < 0$, the material deforms elastically, and the incremental elastic deformation is given by

$$d\varepsilon_{ij}^e=\frac{1+\nu}{E}d\sigma_{ij}-\frac{\nu}{E}d\sigma_{ij}\,\delta_{ij} \qquad i, j=1, 2, 3 \tag{3}$$

b) If $f=k$ and $df=0$, the material deforms both elastically and plastically. In this case, during any increment of stress, the changes of strain are assumed to be divisible into elastic and plastic components.

$$d\varepsilon_{ij}=d\varepsilon_{ij}^{e}+d\varepsilon_{ij}^{p} \tag{4}$$

The plastic strain increment is proportional to the plastic potential and, from the associated flow rule, becomes:

$$d\varepsilon_{ij}^{p}=d\lambda\frac{\partial f}{\partial\sigma_{ij}}=\lambda\left\{\alpha\delta_{ij}+\frac{S_{ij}}{2\sqrt{J_{2D}}}\right\} \tag{5}$$

where: $d\lambda$=a scalar positive function of σ_{ij} and ε_{ij}

δ_{ij}=Kronecker's delta

S_{ij}=deviatoric stress tensor

Substituting equations (3) and (5) into equation (4) yields

$$d\varepsilon_{ij}=\frac{1+\nu}{E}d\sigma_{ij}-\frac{\nu}{E}d\sigma_{ij}\delta_{ij}+\lambda\left\{\alpha\delta_{ij}+\frac{S_{ij}}{2\sqrt{J_{2D}}}\right\} \tag{6}$$

According to the criterion, a state of stress outside the yield surface is not stable. Thus, a special computational algorithm to bring back the state of stress on the yield surface proposed by Siriwardane and Desai[10] is incorporated in the program. The details of Drucker-Prager yield criterion and the Reye's incremental stress-strain relationship used in the developed program are documented elsewhere[15].

2.2 Stiffness Matrix Storage Scheme

In performing three-dimensional analysis on many engineering problems, the capacity of in-core storage of a computer often limits the size of problem to be solved. In other words, the number of unknowns to be treated is restricted by the capacity of in-core storage. This insufficient in-core storage, at the time of writing the global stiffness matrix, can be handled by using a blocked out-of-core solution scheme.

The blocked out-of-core solution scheme adopted in this study consists of blocking the stiffness matrix and storing all blocks in a peripheral storage. The factorization is performed in a sequential block order by reading previously factored blocks into core for each block to be factored. The solution procedure involves two blocks being simultaneously in-cour. Efficiency of the procedure is enhanced when blocking the equations by writing the non-stiffness data onto peripheral storage during the equation solving steps so that maximum core area is available to the global stiffness arrays. The implementation of the blocked out-of-core algorithm provides a means of solving large systems of equations that will not fit into the main-memory of the computer.

3. Program Validation

The developed three-dimensional finite element computer program was validated against the results from the available model footing tests performed by Badie[2] and Das[5]. Two-dimensional plane-strain and three-dimensional model footing tests were simulated using the

developed three dimensional computer program, and the results were compared for validation purpose. In simulating the two-dimensional plane-strain model footing tests using the developed three-dimensional program, the deformations were constrained to one plane (x-y plane) in order to achieve the plane strain condition. The details of the model footing tests are available elsewhere[2, 5].

Comparisons are made in Figs. 1 and 2 which present footing pressure vs. settlement(p vs. δ) relations obtained from the computer analysis and model footing tests for kaolin and sand, respectively. The kaolin, a commercially available clay, has a median grain size of 0.01 mm and a clay size fraction(<0.002 mm) of about 78%. The liquid limit, plasticity index, and specific gravity of the soil are 58%, 22%, and 2,60, respectively. It is classified as MH according to the Unified Soil Classification system. The soil has a dry unit weight of 14.3kN/m^3 with a water content of 23%. A fine silica sand has the uniformity coefficient, coefficient of gradation, and the effective size of 1.53, 1.1, and 0.34 mm, respectively, with a relative density of 70%. Table 1 summarizes the material properties of the kaolin and the sand used in the computer analysis, which are from Badie[2] and Das[5], respectively.

Table 1. Material properties of test soils and concrete footing

Material Properties	Kaolin	Sand	Concrete Footing
Initial Modulus in compression(kN/m^2)	19,840	5,200	2.27×10^7
Poisson's ratio	0.39	0.30	0.20
Cohesion(kN/m^2)	158.5	0.0	N/A
Internal friction angle(Degree)	8.0	40.3	N/A
Dry unit weight(kN/m^3)	14.3	17.1	24.3

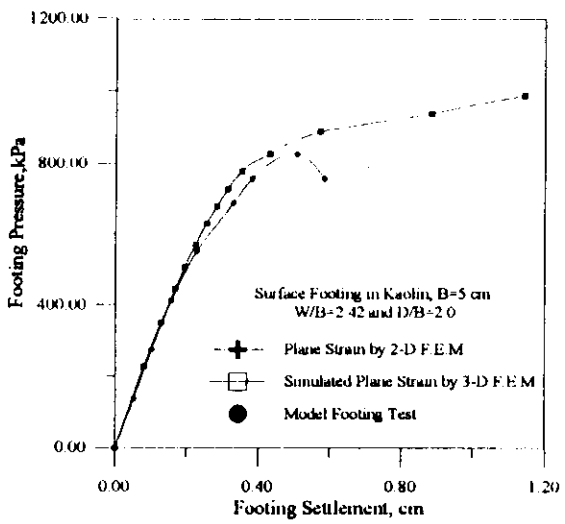

Fig. 1 Comparison of footing pressure vs. settlement curves between finite element analyses and model footing test in kaolin

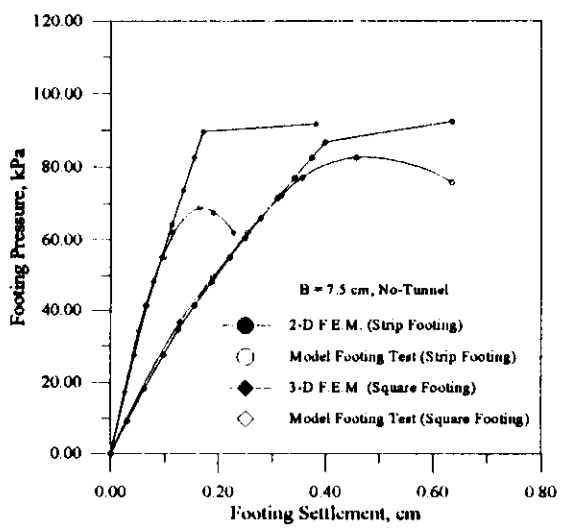

Fig. 2 Comparison of footing pressure vs. settlement curves between finite element analyses and model footing test in sand

Fig. 1 contains three sets of dta: they are the data obtained from the simulted plane strin analysis by the three−dimensionaal finite element program, the two−dimensional finite element program, aand the model footing test for a 5cm wide strip footing in kaolin located avove a tunnel having W/B=2.42 and D/B=2.0 There are four sets of data in Fig. 2' two sets are the results of computer analyses nd the other two are the results of model footing tests for a 7.5cm wide strip and a 7.5cm wide square footings. As seen in Fig. 1, the computer generaated p vs. δ curves compare fairly well with the model test data. The comparison in Fig. 2 between the computer anlyses and the model footing tests results in sand shows very good agreement between the two sets of data for the strip footing. For the square footing, the two curves aalso match very well except at the final stage of loading. The exact cause for such discrepncy is not known. Based on the comparison, the developed computer program appears to be capable of describing the ghree dimensional stress and deformation behavior of fooing−soil−tunnel system.

4. Finite Element Analysis

In the analysis of square footing-unlined tunnel system, a 0.9m-wide reinforced concrete square footing and a circular continuous unlined tunnel which is parallel and centered with the footing axis are considered. The conditions analyzed here are limited to the conditions in the plane tunnel section away from the tunnel heading. Although, in practice, the unlined portion of a soft ground tunnel has a limited length, the continuous unlined tunnel was considered in this study in an attempt to obtain lower bound stability solutions for the footing-tunnel system. The supporting soil used in the analysis is a kaolin which is commercially available under the name Edgar Plastic Kaolin(EPK). In the finite element analysis, the entire footing-soil-tunnel system was represented as an assemblage of a finite number of 8-node hexahedaral elements interconnected by a finite number of nodal points. The vertical and horizontal boundaries of the finite element meshes were placed at 10 and 9 times the footing width from the footing center and base, respectively. These locations were selected through a preliminary analysis such that they would have insignificant effect on the results of finite element analysis. A typical finite element mesh is shown in Fig. 3.

In simulating the footing and tunnel interaction, the soil and the footing pressures were applied in increments to the final configuration of the tunnel. This approach was adopted in order to investigate the ultimate bearing capacity behavior of the footing located above unlined tunnel and the response of unlined tunnel to surface loading. The pre and post-processing was done on a 486-Based PC: an IBM RISC 6000/350 workstation was used for the finite element computer analysis. The results of analysis are discussed in the subsequent paragraphs.

4.1 Ultimate Bearing Capacity

The performance of a square footing located above an unlined tunnel was investigated using the ultimate bearing capacity of the footing. The ultimate bearing capacity values for

the conditions analyzed were determined from the computer generated footing pressure vs. footing settlement(p *vs.* δ) and footing pressure vs. area of yielded elements(p *vs.* yld) relations. The detailed criterion for ultimate bearing capacity determination used in this study is available elsewhere[15]. In the analysis, the ultimate bearing capacity values of the footings with tunnel(q_t) are normalized with that of no-tunnel condition(q_{nt}), and a non-dimensional ratio(q_t/q_{nt}) is used. These values are then graphically related with the various influencing factors such as tunnel size(W) and depth(D), and footing embedment depth (D_f).

The effect of D/B on the ultimate bearing capacity of a square footing located above a tunnel is presented in Fig. 4. Included are the curves for two levels each of D_f/B and W/B. As would be expected, the ultimate bearing capacity increases with increasing D/B for all levels of tunnel size and footing embedment, reaching the value of no-tunnel condition at a certain value of D/B[$(D/B)_{cr}$]. The values of $(D/B)_{cr}$, named critical depth hereinafter, vary with tunnel size, as expected, but appear to be almost constant with the level of footing embedment, suggesting that the footing embedment depth has insignificant effect on $(D/B)_{cr}$.

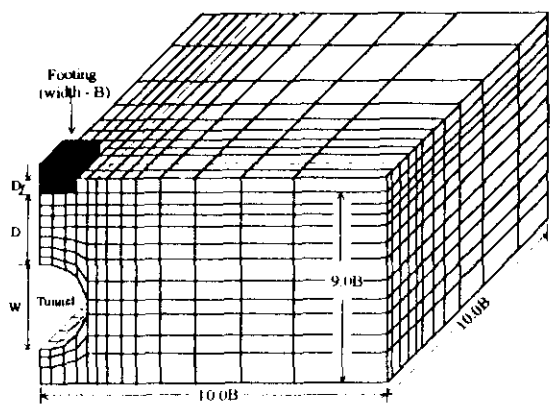

Fig. 3 A typical finite element mesh used in the computer analysis

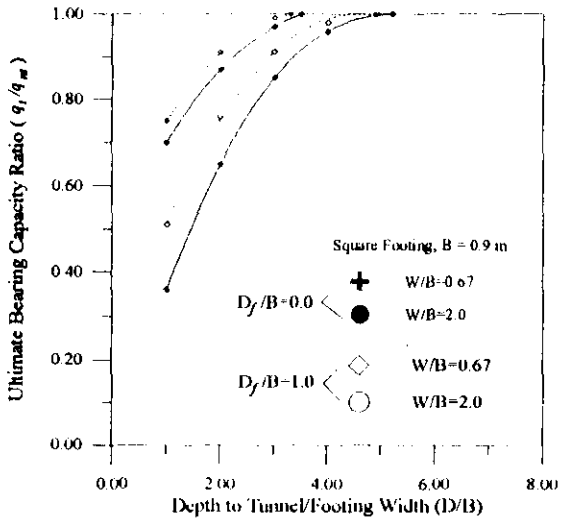

Fig. 4 Variation of ultimate bearing capacity ratio with D/B fora square footing

Fig. 5 presents the variation of ultimate bearing capacity with tunnel size(W) for strip and square surface footings. As expected, the ultimate bearing capacity decreases as W/B increases or D/B decreases. A direct comparison between the curves for strip and square footings, indicates that for a given D/B and W/B, the ultimate bearing capacity ratio for the square footing is always higher than that for the strip footing, and that the difference becomes greater for larger and shallower tunnels. Smaller bearing capacity ratio for square

footings in fact suggests not only greater bearing capacity for the square than the strip footings but the fact that the tunnel effect on the square footing is smaller. For example, for W/B=2.0 and D/B=2.0, the ultimate bearing capacity for the square and the strip footings are approximately equal to 990 kPa[$q_f=0.65\times(q_{ult})_{square}$] and 720 kPa[$q_f=0.60\times(q_{ult})_{strip}$], respectively. When no tunnel exists, the computed bearing capacity values are 1524 kPa and 1200 kPa for the square and the strip footings respectively. The ratio of q_{square}/q_{strip} is greater for with tunnel condition than without tunnel condition: i.e., 1.38 vs. 1.27. This trend, which may be due to the three dimensional effect, demonstrates that the effect of footing shape on the ultimate bearing capacity of a footing is more pronounced when a tunnel is present.

The variations of ultimate bearing capacity ratio with D_f/B are shown in Fig. 6 for two levels of W/B. It is seen that with increasing footing embedment depth, the bearing capacity ratio also increases, which is in turn suggesting diminishing tunnel effect on the ultimate bearing capacity with increasing footing embedment depth. This trend may be attributed to the fact that although D/B remains the same for all levels of D_f/B, the overall depth to tunnel measured from the ground surface is greater at higher D_f/B. This would lead to a greater confinement effect on the supporting soil, providing more shearing resistance. Consequently, with other factors being equal, the influence of a tunnel on the footing performance is smaller for footings with higher D_f/B.

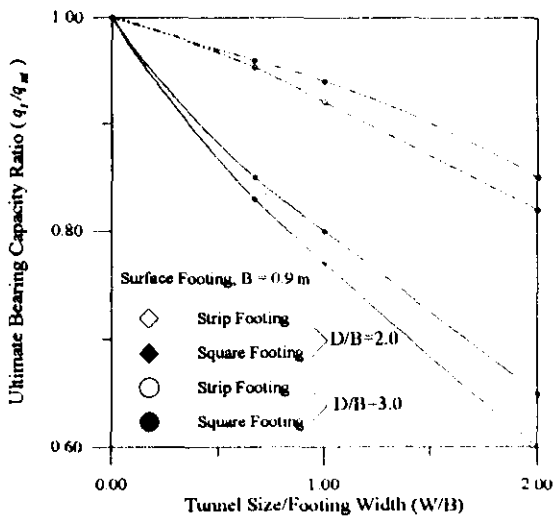

Fig. 5 Variation of ultimate bearing capacity ratio with tunnel size for a strip and a square surface footings

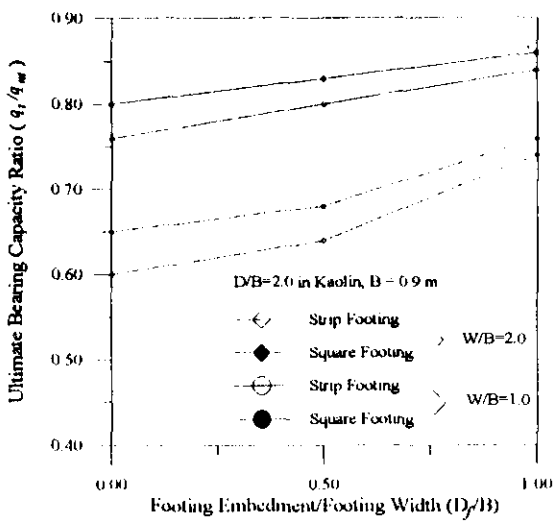

Fig. 6 Variation of ultimate bearing capacity ratio with D_f/B for a strip and a square footings

4.2 Stress Distribution

Stress distributions in the foundation soil and around the tunnel perimeter for a con-

dition with a tunnel centered under a square footing are investigated to elucidate the response of unlined soft ground tunnel to a footing load. The square footing carries a vertical pressure of 690kN/m^2 and the tunnel has W/B=2.0 and D/B=2.0. Also presented are those under a strip footing carrying the same vertical pressure. The vertical pressure of 690kN/m^2 is well below the ultimate bearing capacities of the footings.

Fig. 7 shows the vertical stress distributions on various vertical planes. The vertical planes considered are at the tunnel center, at the tunnel edge, and at 8.0B away from the footing center. It is seen that due to the arching support mechanism, the vertical stress is transferred away from the tunnel crown toward the tunnel spring line. As expected, the stress intensities under the square footing are generally lower than those under the strip footing as much as 22%. For the plane at tunnel center, the greatest difference takes place somewhere around the mid-height between the footing base and the tunnel crown. Near the tunnel crown, the difference becomes negligible as the vertical stress takes zero value due to the inward crown settlement. Along the plane at tunnel edge, however, the difference increases with depth and becomes maximum at the tunnel spring line. On the vertical plane at 8.0B away from the footing center, essentially no difference is seen primarily because the vertical stress is induced mainly by soil weight with little or no influence of footing pressure.

The vertical, horizontal, and shear stresses around the tunnel periphery are presented in Fig. 8. The stresses are taken from the elements surrounding the tunnel perimeter and are plotted against the central angle measured clockwise from the tunnel crown. As seen, the maximum vertical stress, which is approximately 46% of the total load(earth pressure and footing load), occurs at the tunnel spring line due primary to the arching support mechanism, while the maximum shear stress occurs near the tunnel shoulder. Note that the maximum horizontal stress is tensile at the crown, and the zone between approximately $\pm 20^\circ$ from the tunnel crown is subjected to a tensile horizontal stress. Comparison of the stress distributions between the strip and the square footing cases reveals that the difference between the two cases are confined within the upper half of the tunnel with the maximum values of each stress developed under the square footing being approximately 90%, 79%, and 74% for vertical, shear, and horizontal stresses, respectively, of those under the strip footing. Based on these stress distributions, it can be expected that the stress distribution around the lower half of tunnel is not significantly affected by the footing shape.

The variations of tangential and radial stresses around the tunnel perimeter with the plane location(measured in the direction of tunnel axis) are presented in Fig. 9. The planes under consideration are located at the footing center(z=0.0), near the footing edge(z=0.5B), and approximately at eight times the footing width from the footing center(z=8.0B). Note that the tunnel crown is subjected to a considerable magnitude of tensile tangential stress at the section immediately below the footing center, due to the inward soil movement into the tunnel. The tangential stress then becomes compressive as it rotates from the crown and exhibits a maximum value in the region between the shoulder and spr-

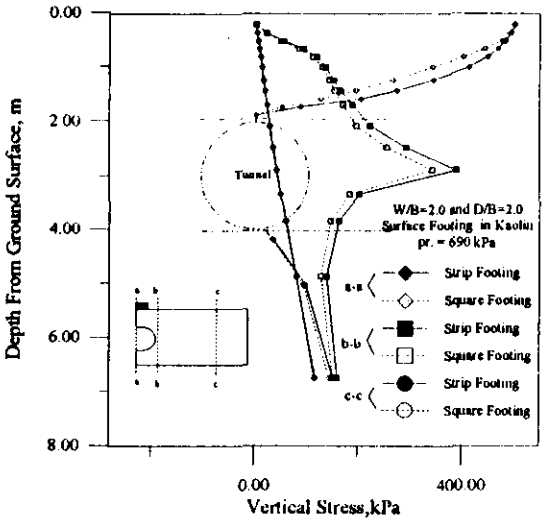

Fig. 7 Vertical stress distributions in the foundation soil for W/B=2.0 and D/B=2.0

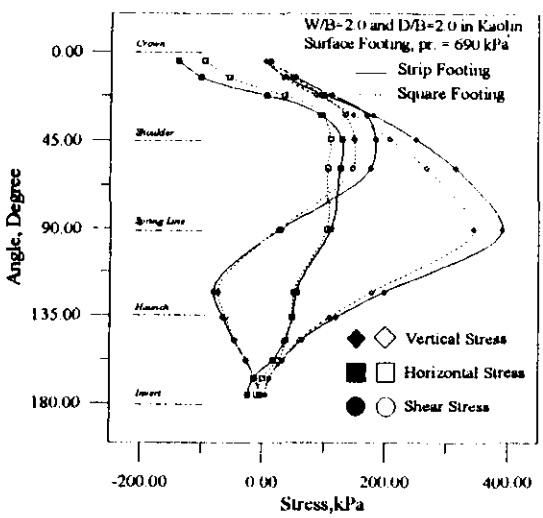

Fig. 8 Stresses in the elements along tunnel perimeter for W/B=2.0 and D/B=2.0

ing line. It is shown that the maximum tangential stress at the section b-b is approximately 86% of that at the section a-a. At the section c-c, the tangential stress becomes considerably smaller with the pattern similar to that due to soil weight only, indicating very little influence of footing load at this section. The radial stresses around the tunnel periphery at the sections close to the footing are very small except in the region between shoulder and haunch, where the outward tunnel deformation takes place. Unlike the tangential stress, the variation of radial stress with plane location is not as pronounced due to the traction free nature of tunnel. From this trend, it is expected that the tunnel experiences higher tangential stress gradient along the tunnel axis than the radial stress when loaded with a square footing.

4.3 Footing Settlement and Tunnel Deformation

When an unlined tunnel is loaded with a footing, interaction between the two may result in a considerable magnitude of footing settlement and tunnel deformation depending on the degree of the interaction. To ensure both footing and tunnel stability, the footing settlement and tunnel deformation behavior must be fully understood. The following paragraphs present discussions on footing settlement and tunnel deformation behavior.

Fig. 10 illustrates footing pressure vs. footing and tunnel crown settlement relations for W/B=2.0 and D/B=2.0 under a square embedded footing of $D_f/B=0.5$. It is seen that, as would be expected, the footing settlement is always greater than the crown settlement for a given footing pressure. This is because when a footing is constructed on the ground with a tunnel, the footing settlement results from the soil compression as well as the tunnel deformation. One interesting trend shown in this figure is that for the shallow tunnel

(D/B=2.0) the footing pressure causing tunnel collapse(tunnel collapse pressure) appears to be approximately the same as the ultimate bearing capacity of the footing.

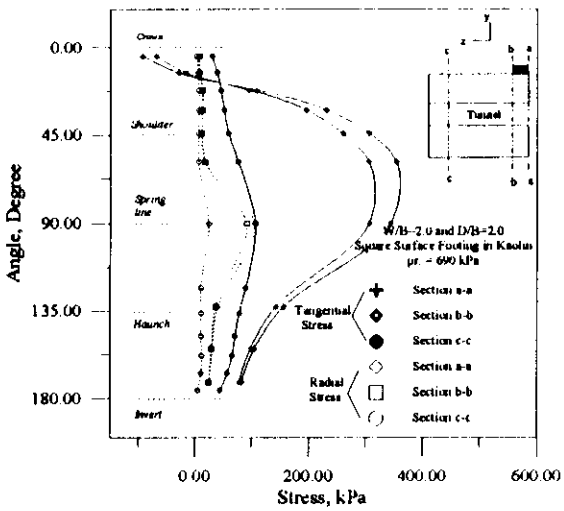

Fig. 9 Tangential and Radial stresses in the elements along tunnel perimeter at various planes along tunnel axis for 0 and D/B=2.0

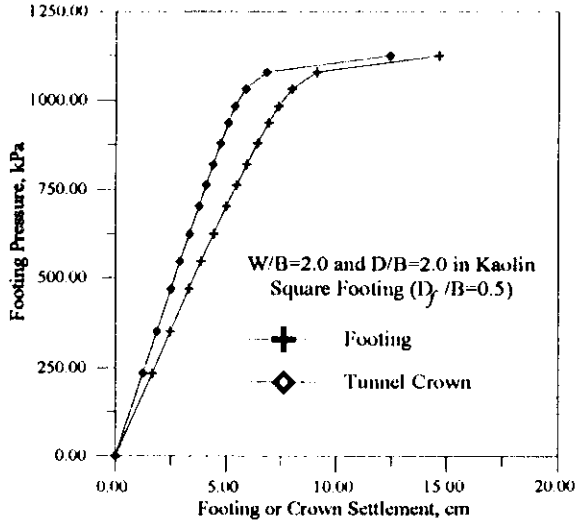

Fig. 10 Footing pressure vs. footing and crown settlement relations for W/B=2.0 and D/B=2.0 under a square footing with D_f/B=0.5

Another view of the relation between the footing and the crown settlements is shown in Fig. 11 for a shallow(D/B=2.0) and a deep(D/B=4.0) tunnels. As seen, the crown settlement at a given footing settlement is greater for the shallow tunnel than for the deep tunnel, due primarily to a greater footing and tunnel interaction when the tunnel is located closer to the footing. In addition, it is seen that the curve for the shallow tunnel is much steeper than that for the deep tunnel, and that the slope of the last portion of the curve for the shallow tunnel becomes almost 45° angle indicating that the footing settles at the same rate of crown settlement. The curve for the deep tunnel, however, is much flatter than that for the shallow tunnel and becomes almost horizontal, indicating higher rate of footing settlement than crown settlement. This trend demonstrates that for shallow tunnels, the footing failure is likely caused by tunnel collapse, while shear failure of the supporting soil would be the likelihood of footing failure for the footing with deep tunnel.

Fig. 12 illustrates the variation of crown settlement for a constant footing pressure of 1034kN/m^2 with respect to the depth to tunnel(D) for three tunnel sizes: W/B=0.67, 1.0, and 2.0. As seen, the crown settlement is larger for the larger tunnel for a given D/B and decreases as D/B increases for all tunnel sizes. The rate of decrease, however, varies among different sizes of tunnels and appears to be much faster for the larger tunnel(W/B=2.0) than for the smaller tunnel(W/B=0.67). This is because the influence of the footing load on the tunnel dissipates faster for larger tunnel than for smaller tunnel when D/B increases. Note that the trend of crown settlement with depth to tunnel(D) is somewhat opposite to that for which a tunnel is excavated under an existing footing. This is because the trend

of crown settlement presented here is due to the application of footing load, and consequently, a larger crown settlement results in when the tunnel is located closer to the ground surface due to the greater degree of interaction between the footing and the tunnel.

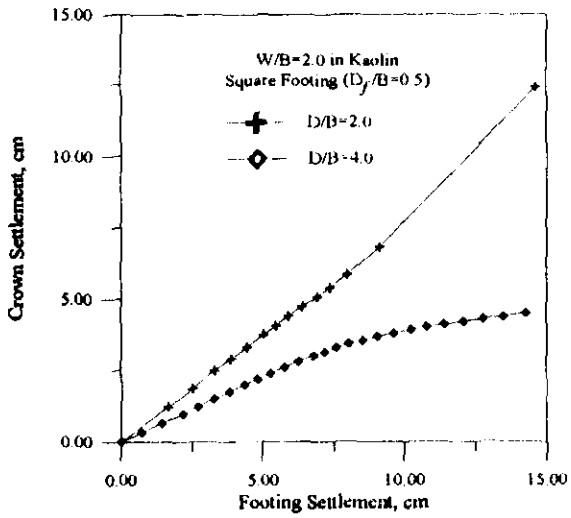

Fig. 11 Footing settlement vs. crown settlement relations for D/B=2.0 and D/B=4.0 with W/B=2.0 under a square footing

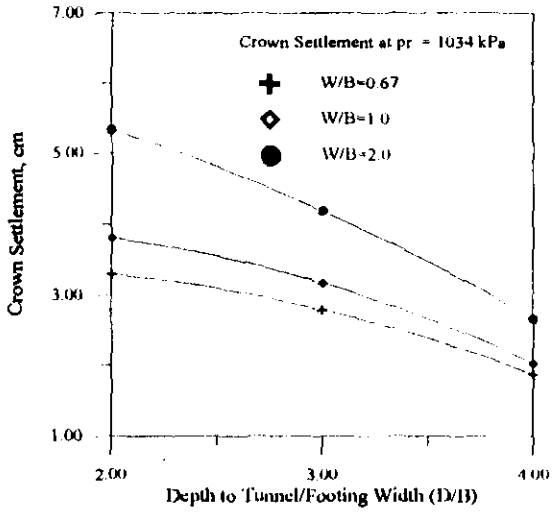

Fig. 12 Variation of crown settlement at a constant footing pressure with D/B

5. Summary and Conclusions

This paper presents the results of a study on the three-dimensional behavior of square footing and unlined soft ground tunnel using a developed three-dimensional finite element computer program. In the analysis, the footing was characterized as a linear elastic material and the foundation soil as a nonlinear elastic perfectly plastic material which obeys Hooke's law and Drucker-Prager yield criterion. The developed computer program was validated against the results of available model footing tests. Various factors considered in the analysis include level of footing embedment, tunnel size, and tunnel location. The analysis was performed on an IBM RISC 6000/350 computer.

The interaction between a footing and an unlined tunnel is simulated by applying the soil and footing pressures in increments to the final configuration of the tunnel. Based on the results of finite element analysis, the interaction mechanism of footing and tunnel was evaluated. Among the behaviors investigated are ultimate bearing capacity, stress distribution, and footing settlement and tunnel deformation. The results show that there is a critical depth of tunnel(D_{cr}) below which the presence of a tunnel does not have influence on the footing performance. The value of D_{cr} varies with tunnel size(W) but appears to be independent of depth of footing embedment(D_f). Also showed is that the effect of footing shape on ultimate bearing capacity is more pronounced when a tunnel is present, and that

the tunnel effect on footing performance is smaller for footings with greater footing embedment depth. It is also revealed that an unlined tunnel under a square footing is subjected to three dimensional stress pattern along the tunnel axis, and that the tangential stress variation along the tunnel axis is more pronounced than the radial stress. The study on footing settlement and tunnel deformation indicates that for shallow tunnels, the footing failure is likely caused by tunnel collapse, while shear failure of the supporting soil would be the likelihood of footing failure for the footing with deep tunnel.

References

1. Azam, G.,(1990). "Stability of Shallow Continuous Footings Supported by Two-Layer Soil Deposits with an Underground Void", Ph.D. Thesis, The Pennsylvania State University, University Park, PA.
2. Badie, A.,(1983). "Stability of Spread Footing Supported by Clay Soil with an Underground Void", Ph.D. Thesis, The Pennsylvania State University, University Park, PA.
3. Baus, R.L.,(1980). "The Stability of Shallow Continuous Footings Located above Voids", Ph.D. Thesis, The Pennsylvania State University, University Park, PA.
4. Beer, G., Watson, J. O., and Swoboda, G.,(1987). "Three-Dimensional Analysis of Tunnels Using Infinite Boundary Elements", Computer and Geotechnics, Vol. pp. 37－58.
5. Das, B. M.,(1993). Personal Communication,
6. Davis, E. H., Gunn, M. J., Mair, R. J., and Seneviratne, H. N.,(1980). "The Stability of Shallow Tunnels and Underground Openings in Cohesive Material", Geotechnique, Vol. 30, No. 4, pp. 397－416.
7. Drucker, D. and Prager, W.,(1952). "Soil Mechanics and Plastic Analysis in Limit Design", Quarterly of Applied Mathematics, Vol. 10, No. 2, pp. 157－165.
8. Duncan, J. M. and Chang, C. Y.,(1970). "Nonlinear Analysis of Stress and Strain in Soils", ASCE Journal of Soil Mechanics and Foundation Division, Vol. 96, No. 5, pp. 1629－1653.
9. Lee, K. M. and Rowe, R. K.,(1990). "Finite Element Modelling of the Three-Dimensional Ground Deformations Due to Tunnelling in Soft Cohesive Soils: Part Ⅱ-Results", Computers and Geotechnics, Vol. 10, pp. 111－138.
10. Siriwardane, H. J. and Desai, C. S.,(1983). "Computational Procedures for Non-linear Three-Dimensional Analysis with Some Advanced Constitutive Laws", International Journal of Numerical and Analytical Methods in Geomechanics, Vol. 7, No. 2, pp. 143－171.
11. Wang, M. C., Yoo, C. S., and Hsieh, C. W.,(1989). "Effect of Void on Footing Behavior under Eccentric and Inclined Loads", Proceedings, Foundation Engineering: Current Principles and Practices, ASCE, Vol. 2, pp. 1226－1239.
12. Wang, M. C. and Hsieh, C. W.,(1992). "A Bearing Capacity Determination Method for Strip Footing Underlain by Void", Transportation Research Board, 71st Annual Meeting, Washington D. C.
13. Wood, L. A. and Larnach, W. L.,(1985). "The Behavior of Footings Located above Voids", Proceedings, Eleventh International Conference on Soil Mechanics and Foundation Engineering, San Francisco, Vol. 4, pp. 2273－2276.
14. Yoo, C. S.,(1987). "Effect of Void on Stability of Strip Footing Subjected to Eccentric and Inclined Loading", Master of Engineering Report, The Pennsylvania State University, University Park, PA.
15. Yoo, C. S.,(1993). "Interaction Between Shallow Foundations and Unlined Soft Ground Tunnels", Ph.D. Thesis, The Pennsylvania State University, University Park, PA.

(접수일자 1994. 6. 17)